ARTICLE

Check for
updates

Optimal Design of Porous Media in Solar Vapor Generators by Carbon Fiber Bundles

Mohammad Yaghoub Abdollahzadeh Jamalabadi and Jinxiang Xi*

Department of Biomedical Engineering, University of Massachusetts, Lowell, MA, USA

*Corresponding Author: Jinxiang Xi. Email: Jinxiang_Xi@uml.edu

ABSTRACT

As a means of harvesting solar energy for water treatment, solar-driven vapor generation is becoming more appealing. Due to their entangled fibrous networks and high surface area, fibers can be used as building blocks to generate water vapor. In this paper, using a two-dimensional fiber bundle model, we studied the generation of solar vapor based on the fiber height, distance between fibers, and input sun radiation. The performance of solar absorption system was also evaluated by evaluating thermal and water management. Results showed a constant increase in solar vapor generation with an increasing fiber height and decreasing inter-fiber distance. However, the gain rate of using taller and more densely packed fiber bundles dwindled quickly. On the other hand, a shorter fiber had a higher evaporation rate per fiber height. The distance between fibers had a nonlinear effect on the fiber bundle evaporation rate. A new fiber bundle design was recommended with a fiber height of 15–20 mm and an inter-fiber distance of 1.5 mm. The results of this study can provide guidelines for future fiber bundle designs with increased efficiency, reduced cost, and versatile applications (i.e., desalination, water purification, and power generation).

KEYWORDS

Solar vapor generation; porous structures; thermal management; water management; drying process

Nomenclature

A	Surface area of sample, m^2
a	Thermal diffusion coefficient, $m^2 s^{-1}$
c	Specific heat, $J\,kg^{-1}K^{-1}$
d	Fiber diameter, m
D	Distance between fibers, m
D_a	Air diffusion coefficient, $m^2 s^{-1}$
D_v	Vapor diffusion coefficient in air, $m^2 s^{-1}$
h	Fiber height, m
H	Channel height, m
h_t	Convective heat transfer coefficient, $W\,m^{-2}K^{-1}$
h_{fg}	Latent heat of vaporization, $J\,kg^{-1}$
h_m	Convective mass transfer coefficient, $m\,s^{-1}$

M	Moisture content, kg kg^{-1}d.b.
P_v	Vapor pressure, Pa
q_w	Sun radiation power, W/m^2
R_g	Universal gas constant, J mol^{-1}K^{-1}
RH	Relative humidity of air, %
T_0	Initial temperature, K
T_a	Drying air temperature, K
u_a	Velocity of air, m s^{-1}

Greek symbols

λ	Thermal conductivity, W m^{-1} K^{-1}
ρ	Density, kg m^{-3}
ρ_a	Density of air, kg m^{-3}
τ	Time, s
μ_a	Dynamic viscosity of air, N s m^{-2}
ν_a	Kinematic viscosity of air, m^2 s^{-1}

1 Introduction

Solar energy is a serious competitor to conventional power generation when the in-direct costs of fossil fuels are considered. Thus, processing sunlight via an absorbing system is an important method of generating clean energy. Almasoud et al. [1] studied the future of solar energy in Saudi Arabia and suggested that solar energy would have a lower cost than fossil fuel energy. Considering the costs associated with environmental and health damage. Bae et al. [2] investigated the use of flexible thin-film black gold membranes with ultra-broadband plasmonic nanofocusing to generate solar vapor efficiently and found a new structure that has a variety of applications in solar energy harvesting, thermos-plasmonics and related technologies.

Cellulose derivatives are useful in improving the porous structure. With the use of water and cellulose derivatives, Bella et al. [3] proposed a novel approach to truly sustainable solar cells. In another study, Bella et al. [4] developed ultra-breathable and protective carbon nanotube membranes with sub-nanometer pores and reported their new device has low cost, environmental compatibility, appreciable efficiency, long-term durability, and enhanced safety. The process of vaporization was examined by Brrindle [5]. Using Sample Introduction Systems in ICPMS and ICPOES, they found that vapor generation had evolved from something that required separate equipment (especially for hydride-forming elements, such as As, Se, Sb, Te, and atomic Hg) to volatile species. In addition, they demonstrated that vapor generation can be useful for the analysis of speciation in certain circumstances. Chen et al. [6] investigated a floating solar concentrated distillation configuration and reported significant effects of surface optical parameters and incidence angles on solar energy harvesting. The thermodynamic model and experimental results were then used to determine the heat convection and heat-mass transfer relationships. Ge et al. [7] investigated solar steam generation and developed a porous conducting polymer hydrogel to generate solar steam. It consumes less energy to evaporate due to the activation of PSS part to water molecules by polymer-water interaction.

Heat localization in textiles is a way to improve heat and mass transfer through bundles. According to Ghasemi [8], solar steam is generated by heat localization. A textile waste-derived cellulose-based composite aerogel for efficient solar steam generation was investigated by He et al. [9]. Due to their renewable biopolymer resources and interconnected micropores, cellulose-based aerogels have

been deemed promising candidates for solar steam generation. He et al. [10] also investigated the feasibility of manufacturing polydopamine nanosphere-decorated fabrics for solar steam generation. The synthesis of sea urchin-like carbon from metal-organic frameworks for the production of advanced solar vapor generators was introduced by He et al. [11]. By facilely coating natural wood with carbon materials that have been pyrolyzed from sea urchin-like metal and organic frameworks (MOFs), they were able to prepare a bilayer solar evaporator. Another aspect of wood is that not only does it provide abundant hydrophilic channels for water supply, it also significantly reduces the enthalpy of water evaporation through hydrogen bonds between water molecules and the hydrophilic channels in the wood. Ito et al. [12] used multifunctional porous graphene as a heat generator for steam generation and demonstrated an energy conversion of 80% by heat localization. Kalogirou [13] investigated seawater desalination using renewable energy sources and proposed general guidelines for the selection of desalination and renewable energy systems. Li et al. [14] investigated the Ti3C2 as an effective light-to-heat conversion material in two dimensions. Using vapor phase infiltration of carbon, Li et al. [15] analyzed densified aligned carbon nanotube films in a single step by the combination of the chemical vapor deposition and chemical vapor infiltration processes. In order to develop an environmentally safe and renewable solar vapor generation device, Lim et al. [16] investigated the use of agar hydrogel (AHG) and Prussian blue (PB) immobilized on cellulose nanofiber (CNF) for solar evaporation.

Mass transfer improvement through the fiber bundle has been demonstrated to be achieved using nano structures. Linic et al. [17] investigated the efficiency of solar conversion to chemical energy using plasmonic metal nanostructures. Their research leads to efficient nanostructures for the conversion of solar energy. Liu et al. [18] investigated the use of wood graphene oxide composites for the generation and desalination of highly efficient solar steam. They also investigated the controlled growth of super aligned carbon nanotube arrays for the purpose of producing continuous sheets with tenable physical properties [19]. Their product leads to efficient nanostructures for distillation applications. Bioinspired design of electro spun nanofiber-based aerogel for cost-effective and efficient generation of solar vapor was examined by Liu et al. [20]. Using an ecofriendly crosslinking and freeze-drying method, luffa-inspired electro spun polyacrylonitrile/carbon nanotubes (PAN/CNTs) nanofiber-based aerogels were designed and fabricated. Clean water can be efficiently produced by using this scalable, eco-friendly, and cost-effective aerogel. Bioinspired, reusable, paper-based system was also explored by Liu et al. [21] for high-performance large-scale evaporation. Ma et al. [22] investigated the transport of water inside carbon nanotubes. An umbrella evaporator was proposed for simultaneous vapor generation and salt harvesting based on the mechanism for double sided evaporation, as well as for salt nucleation, growth, and falling.

The fluid flow inside the bundles improves the heat and mass transfer through the fiber bundles. Enhanced flow in carbon nanotubes was investigated by Majumder et al. [23]. Such a novel design can be used in fiber solar applications. Mizuno [24] investigated a graphene black body absorber made of vertically aligned single-walled carbon nanotubes with increased solar absorption. Cancilla et al. [25] studied hydrodynamics and mass transfer in straight fiber bundles with non-uniform porosity, which caused a strong reduction of the Sherwood number. A floating structure with thermal concentration enables steam generation under one sun by Ni et al. [26]. Ni et al. [27] investigated direct vapor generation from nanofluids heated by volumetric ultraviolet radiation. Based on hydrophilic/hydrophobic amphipathic Janus nanofibers, Ouyang et al. [28] proposed a flexible solar absorber that generates vapor efficiently. Electro spun hydrophilic cellulose acetate/hydrophobic polyvinyl butyral amphipathic Janus nanofibers are used as substrates in their study to construct a novel solar absorber. To make the solar absorber, carbon nanotubes, SiO_2 nanoparticles, and polydopamine are modified onto the surface of the Janus nanofiber film. Desalination performance is also promising for the solar

absorber based on Janus nanofibers. Polypyrene-coated cattail fibers are used in the porous biomass foam for photothermal evaporation by Sun et al. [29]. Polypyrene decorated cattail fiber foam is used in this work as a porous solar evaporator. The created foam exhibits a good vapor evaporation rate as well as a photothermal conversion efficiency of 99.6% under one sun illumination.

Novel designs to enhance solar steam generation have been explored in different groups. Using bubbly flow nanofluids and collaborative light-harvesting nanoparticles, Yao et al. [30] studied solar vapor generation using a bubble-flow nanofluid. Their research proposes that a composite nanofluid composed of three different kinds of particles will absorb light over the entire solar spectrum as a composite nanofluid composed of different kinds of particles with distinct absorbance peaks. Furthermore, dynamic bubbles are introduced into the nanofluid to facilitate the generation of solar vapor. Under one-sun irradiation, the bubbly flow nanofluid exhibits the greatest photothermal efficiency of 91.2%, enabling fast vapor diffusion with upward bubble-bursting flow, and thus achieving a decent steam generation efficiency of 40.8%. The extremely black vertically aligned carbon nanotube (VACNT) array was investigated by Yin et al. [31]. Using VACNT arrays, they observed a 10 times faster evaporation rate of water than bare water, a record for solar-thermal-steam generation. Yu et al. [32] investigated the performance of a localized so-lar-driven evaporation system based on surface chemistry. Researchers reviewed current strategies for solving scaling in interfacial solar vapor generation for desalination and brine treatment. Using solar desalination and brine treatment, Zang et al. reduced salt accumulation on evaporators by physical cleaning, ion rejection, and fast ionic diffusion [33]. Zhang et al. [34] investigated the use of carbonized sugarcane as an interfacial photo-thermal evaporator for the generation of vapor. It was demonstrated here that carbonized sugarcane (CSC) can be used as an evaporator. With good hydrophilicity and high solar absorption, the CSC evaporator modified by concentrated nitric acid benefits from the microstructure of CSC. Furthermore, there is evidence that airflow and solar radiation can work together harmoniously to increase evaporation rates.

Integrating fiber research across many disciplines, such as nanofibers, has been explored to increase the efficiency of solar generators. Zhang et al. [35] investigated superlubricity using centimeter-long double-walled carbon nanotubes and showed that superlubricity could be achieved in such nanotubes under ambient conditions rather than under high vacuum. Using 4-inch wafer-scale super-aligned carbon nanotube arrays, Zhang et al. [36] spun and processed continuous yarns that was elastic and could be molded to any desired shape with heat treatment. Zhang et al. [37] demonstrated that the carbon nanotube arrays (CNT) arrays could be tuned from well-aligned, spinnable forests to uniformly wavy, foam-like films by controlling the coalescence of catalyst particles. Zhao et al. [38] explored high-performance salt-resistant solar interfacial evaporation based on plant-inspired design. An eco-friendly device was created from carbon fiber bundles (CFBs). CFBs are held in place by perforated wood, and wood buoyancy keeps the evaporator afloat. This device exhibits ultra-high chemical stability thanks to carbon fibers and wood. However, current fiber bundle designs, especially the selection of the optimal fiber size and the distance between fibers in the bundle, still largely rely on empirical approaches. Due to the complex multi-physics involved in this process, quantitative analyses of fiber bundle designs are still scarce [39–41].

An improved way of optimal design of porous media to the solar vapor generators is desired so that microfiber bundles outcome can be achieved and adverse side effects can be minimized. However, systemic investigations of the fiber bundle designs are scarce, mainly due to the complex multi-physics involved in this application. The objective of this study is to numerically quantify the optimal design of porous media with thermal radiation in various microfiber bundles model geometries. Specific aims include:

(1) to develop a computational model of solar vapor generators in various geometries.

(2) to understand the mass transfer responses of varying bundle geometries to thermal radiation from the sky.

(3) to predict the water mass content in the various geometries under various boundary conditions.

The results of this study will provide insights into the solar vapor generation that can be expected from porous design strategies for fiber bundles.

2 Materials and Methods

Physics involved in this study included radiation from the sun to the CFB, capillary rise within the CFB, diffusion of liquid and gas phases within the CFB, evaporation, and convection. Influencing properties are emissivity, mass-diffusivity of the fiber, contact angle (liquid-solid) and solar illumination or a specific temperature. Parameters of input are height (h), fiber diameter (d), distance between fibers (D) and parameter of interest is evaporation rate (see Fig. 1a).
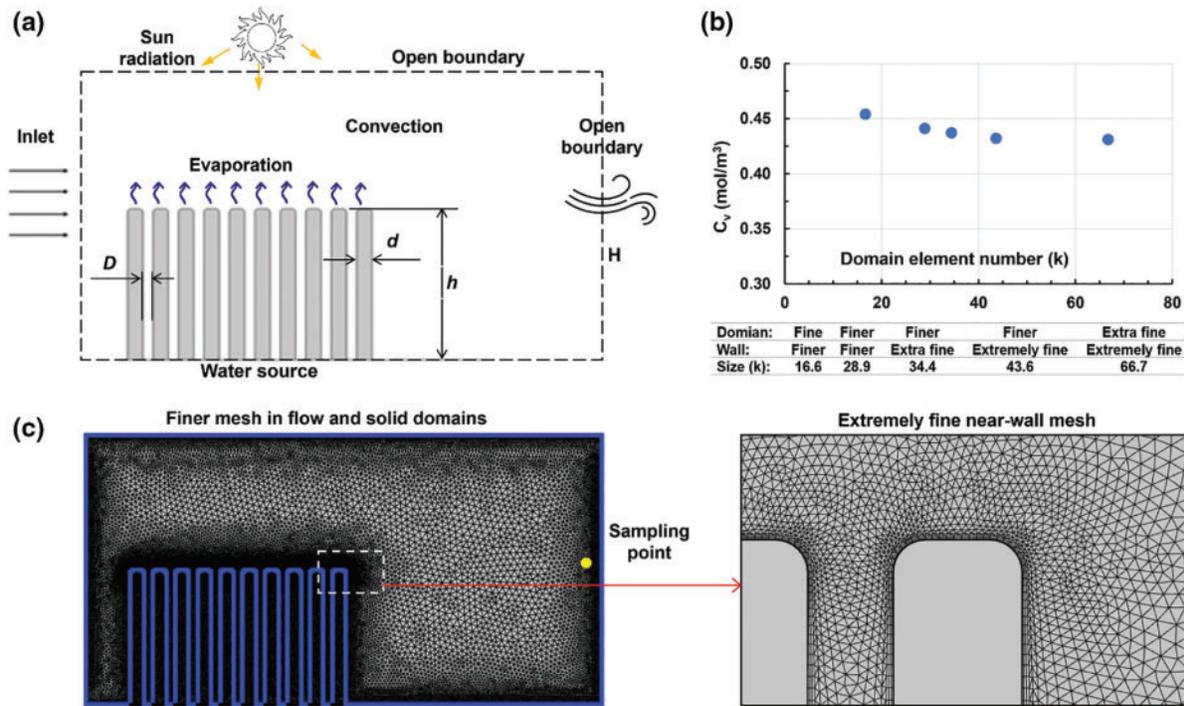
Figure 1: Geometry and computational mesh of the problem: (a) diagram, (b) mesh sensitivity study in term of vapor concentration at the exit, and (c) computational mesh with 43.6 thousand elements

The phase balance between gas and liquid can be written as:

$$S_g + S_l = 1 \tag{1}$$

The index g represents the gaseous phase (in this case, moist air) and the index l represents the liquid phase (in this case, water). Due to the small liquid phase velocity in comparison to the moist air velocity, Darcy's law must be applied to the gas phase pressure gradient to calculate the water velocity u_l.

$$\mathbf{u}_1 = -\frac{\kappa \kappa_r}{S_1 \varepsilon \mu_w} \nabla p_g \tag{2}$$

A general equation to the Transport of Diluted Species of water vapor and liquid water in this paper is:

$$\frac{\partial c}{\partial t} + \nabla \cdot \mathbf{N} = R \tag{3}$$

The correlation for the porosity ε water concentration c_w and liquid phase saturation S_l is:

$$S_1 = \frac{c_w M_w}{\rho_w^\varepsilon} \tag{4}$$

A Millington and Quirk correlation used for effective diffusivity is:

$$D_{\text{eff}} = D_{\text{va}} \varepsilon^{4/3} S_g^{10/3} \tag{5}$$

where $D_{\text{va}} = 2.6 \cdot 10^{-5}\,\mathrm{m^2/s}$. The amount of evaporated water is defined as:

$$m_{\text{vap}} = K \cdot (a_w c_{\text{sat}} - c) \tag{6}$$

where K (SI unit: 1/s) is the evaporation rate, a_w is the water activity ($a_w = 0.91$ hereof), c is the current vapor concentration, and c_{sat} is the saturation concentration of the vapor, which is calculated as:

$$c_{\text{sat}\sim} = \frac{p_{\text{sat}}(T)}{R T} \tag{7}$$

The governing equations for the fluid flow in the porous layer are based on the Darcy's law, as shown in Eq. (2). The governing equations for the moist air in the ambient space were solved with laminar Navier-Stokes flow model,

$$\nabla u = 0; \frac{\partial \mathbf{u}}{\partial t} + u^\blacktriangledown \nabla u = -\frac{1}{\rho} \nabla p + g + \frac{1}{\rho} \nabla^\blacktriangledown \tau \tag{8}$$

where p is the pressure and τ is the deviatoric stress tensor. The local energy balance is:

$$\rho C \frac{\partial T}{\partial t} = \frac{\partial}{\partial x}\left(k_e \frac{\partial T}{dx}\right) + \frac{\partial}{\partial y}\left(k_e \frac{\partial T}{dy}\right) + S \tag{9}$$

The mass balance of vapor in air is:

$$\frac{\partial C_v}{\partial t} = \frac{\partial}{\partial x}\left(D_a \frac{\partial C_v}{dx}\right) + \frac{\partial}{\partial y}\left(D_a \frac{\partial C_v}{dy}\right) + m_{evap} \tag{10}$$

The mass balance of water in porous media is:

$$\frac{\partial C_w}{\partial t} = \frac{\partial}{\partial x}\left(D_w \frac{\partial C_w}{dx}\right) + \frac{\partial}{\partial y}\left(D_w \frac{\partial C_w}{dy}\right) - m_{evap} \tag{11}$$

In this study, the computational model is investigated numerically using COMSOL Multiphysics. For this purpose, we simulated the near surface evaporation under convection and sun radiation over surfaces while temperature and pressure could change inside the fibers. Laminar flow was assumed for the convection of moist air, and multiphase heat transfer was simulated with sun radiation (heat source) and phase-change-induced latent heat (heat sink). The mass transfer of liquid and vapor within the fiber and that of the vapor within the air were simulated using dilute chemical species diffusion.

Regarding boundary conditions, the inlet airflow velocity was specified as 1 m/s; a convection was needed to carry away the solar-generated vapor, which would otherwise accumulate around the fiber bundle due to the much slower diffusion. The ambient relative humidity was 50%. The ambient

temperature ranged from 20°C to 40°C, and the sun radiation intensity q_w ranged from 0 to 800 W/m². The fiber bundle consisted of ten fibers. The fiber diameter ranged from 0.5 to 3 mm, and the fiber length ranged from 5 to 30 mm. The distance between fibers varied from 0.5 to 2.5 mm. Ten fibers were selected in this study based on the balance between two factors: (1) the desire to study vapor generation in different locations of the fiber bundle, *vs.* (2) the increasing computational requirement with more fibers. A selection of ten fibers was found to provide sufficient location sensitivity in evaporation rate while requiring reasonable compactional resources. The initial condition for the vapor concentration inside the fiber was assumed to be the same as the ambient vapor concentration. Grid independence study was conducted by comparing the results among five computational meshes (Fig. 1b). Unser controlled mesh was used in the mesh sequence that domain and boundary mesh sizes could be controlled separately, as shown in the table in Fig. 1b. The vapor concentration at the exit was compared among the five meshes. Less than 1% difference in the vapor concentration (mol/m³) was obtained between the last two meshes, i.e., 43.6 and 66.7 k (Fig. 1b). Therefore, the mesh with 43.6 k was selected for all subsequent numerical simulations and shown in Fig. 1c. For each case, an evaporation time of 5,000 s was simulated. To be computationally efficient, segmental time steps were adopted, which was 0.01 s in the range of 0–5 s, 0.1 s during 5–50 s, 1 s during 50–500 s, and 10 s during 500–5000 s.

3 Results

Fig. 2 presents the vapor concentration for the fiber height h ranging 5–30 mm at d equals to 1.5 mm. As shown by increase of fiber height less humidity received at the last fiber. As well the shorter height helps the fiber bundles to keep their water content (Fig. 2a), which is not desired in this application. A taller fiber bundle at 15 mm expands the moisture through domain and has a better interaction with environment, with a higher vapor concentration in the ambient space (Fig. 2b). Further increasing the fiber height to 30 mm prevents the vapor from reaching the top of the fiber (Fig. 2c), where the vapor can be more easily carried away by convection to make space for further evaporation.
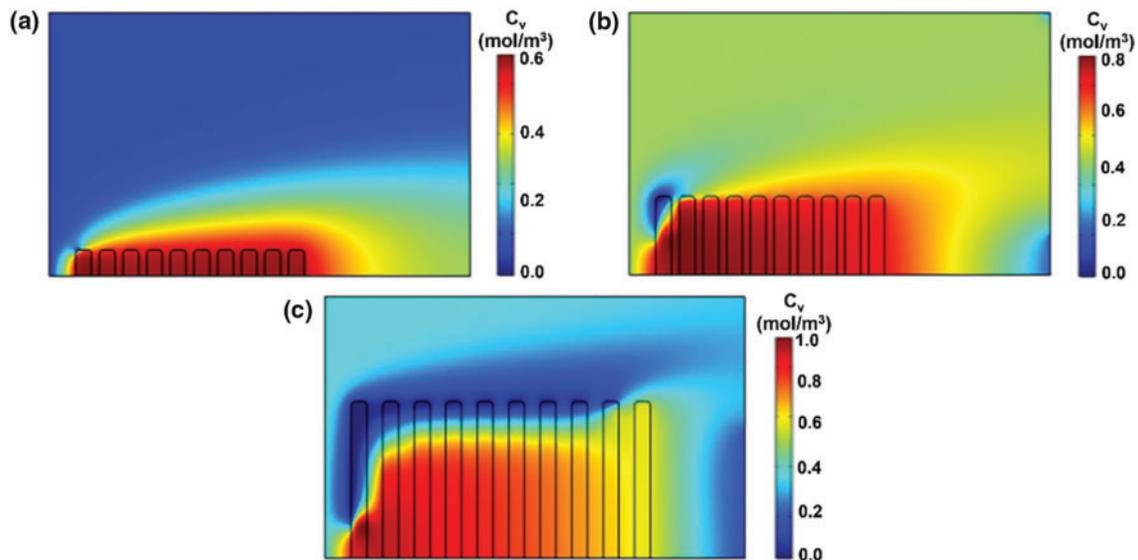
Figure 2: Vapor concentration for (a) h = 5 mm, (b) h = 15 mm, (c) h = 30 mm at d = 1.5 mm

Fig. 3 presents the vapor concentration with different inter-fiber distances D from 0.5 mm to 3 at h = 15 mm. As shown by the increase in the distance, less humidity is received at the last fiber. As well the shorter inter-fiber distances help the fibers to keep their water content which is not desired in this application. Also, the front fibers can be significantly affected by the environmental condition.
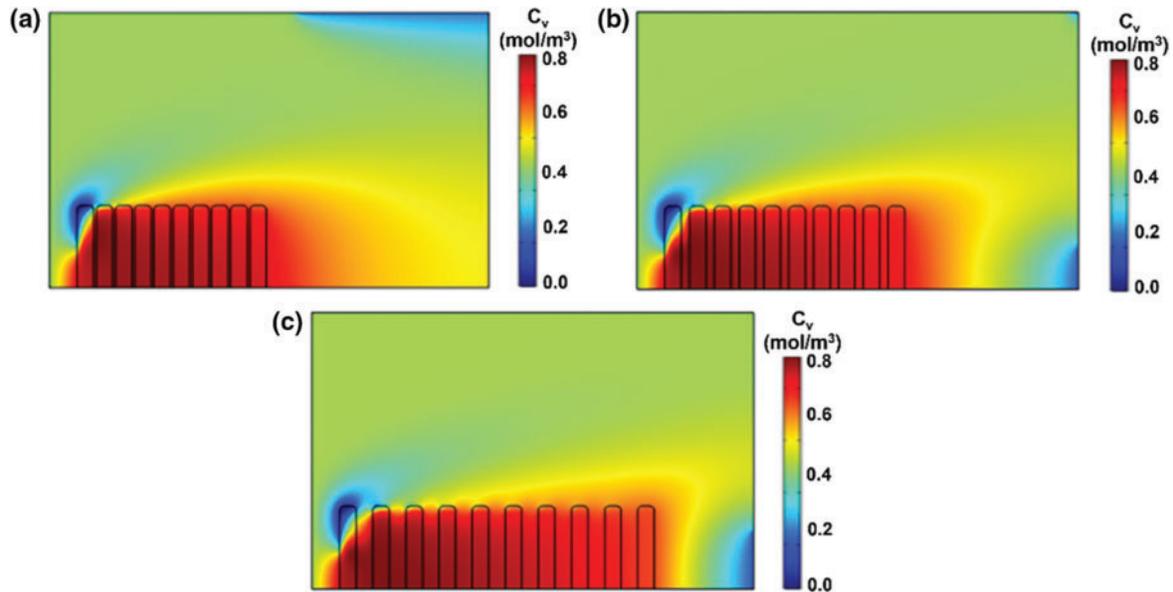
Figure 3: Vapor concentration for (a) D = 0.5 mm, (b) D = 1.5 mm, (c) D = 3 mm at h = 15 mm

Fig. 4 presents the vapor concentration c_v along the fiber for varying fiber bundles with a height h ranging from 5 to 30 mm. The distance between fibers, D is 1.5 mm. Specifically, the c_v variations in the first bundle, middle bundle, and last bundle are shown in Figs. 3a–3c, respectively. Overall, the vapor concentration within a single fiber decreases with increasing fiber height (Y). The vapor concentration continues at a constant level, and after some height, it quickly decreases. This is because evaporation occurs at the fiber surface, which is stronger at the top (due to convection) and weaker at the lower fiber (due to vapor accumulation up to saturation vapor concentration). This leads to the observed vapor concentration profile that is approximately constant at the lower fiber and then suddenly decreases after reaching a certain height where evaporation becomes more intensified.

Fig. 5 presents the evaporation rate for h from 5 to 30 mm, and D equals to 1.5 mm for first bundle, middle bundle, and last bundle. As shown evaporation rate is maximum at the top of each bundle caused by heat received at the top. Sudden changes in evaporation mass give a big chance to the system for heat and mass transfer exchange. Comparing the differences among the three locations. The first fiber bundle exhibits significant impact from the upstream environment, while the middle and last bundles resemble each other despite discrepancy in magnitude.

Fig. 6 presents the vapor mass content, m_l inside the fiber *vs.* time under varying fiber bundle designs. A significant increase in the vapor mass content m_l is observed with increasing fiber height from 5 to 30 mm (Fig. 6a); by comparison, the m_l variation with the inter-fiber distance is much smaller (Fig. 6b). Fig. 6c compares the final m_l at 5,000 s among fiber bundles with different heights and inter-fiber distances. It is observed that the m_l increases linearly with the fiber height h till 20 mm and then increases at a lower rate after 20 mm. Moreover, the m_l varies nonlinearly with the distance between fibers. The final mass inside the fiber increases as the inter-fiber distance increases from 0,5 to 2.5 mm.

This is presumably attributed to the reduced evaporation from a more densely packed bungle (0.5 mm herein), thus leaving more vapor mass inside the fibers.
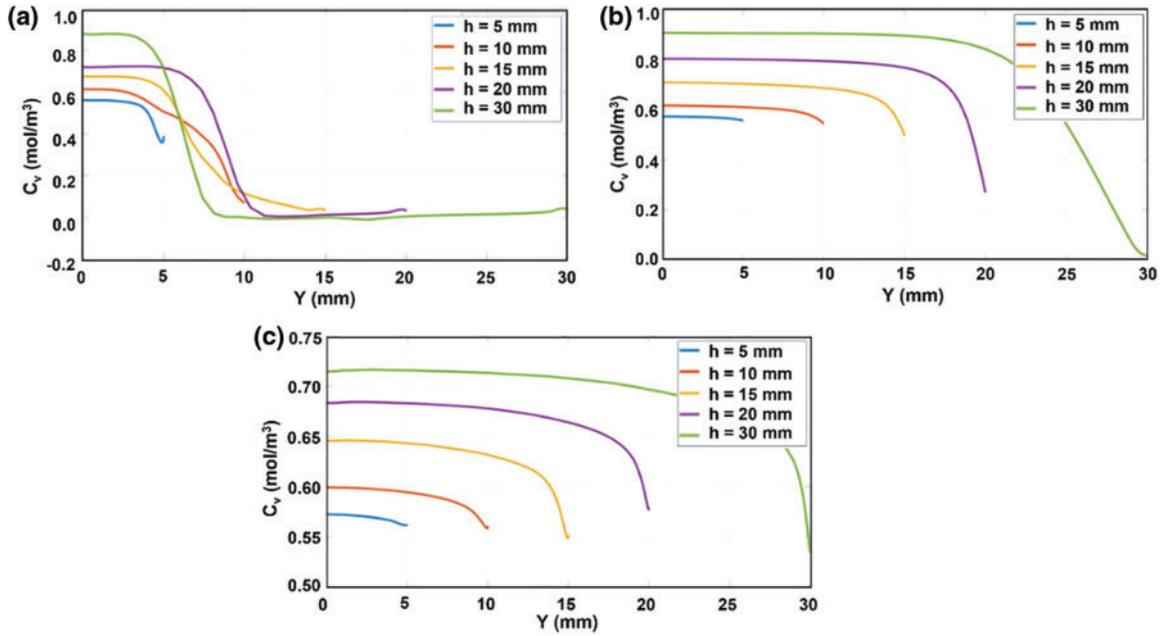
Figure 4: Vapor concentration for h = 5, 10, 15, 20, 30 mm and D = 1.5 mm for (a) first bundle, (b) middle bundle, (c) last bundle
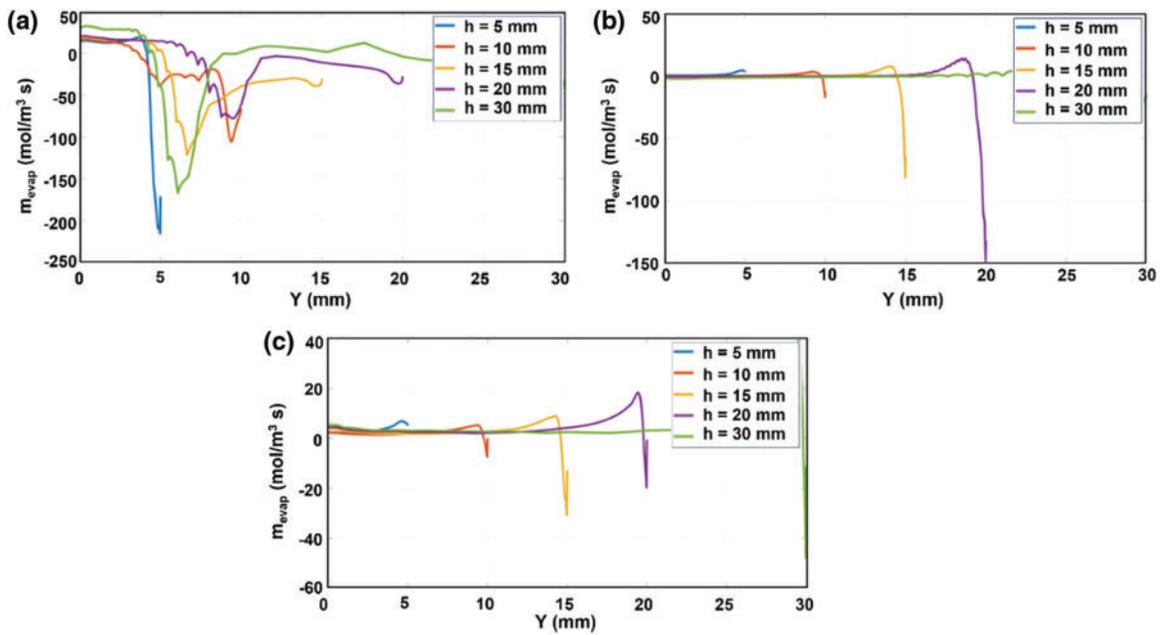
Figure 5: Evaporation rate for h = 5, 10, 15, 20, 30 mm and D = 1.5 mm for (a) first bundle, (b) middle bundle, (c) last bundle
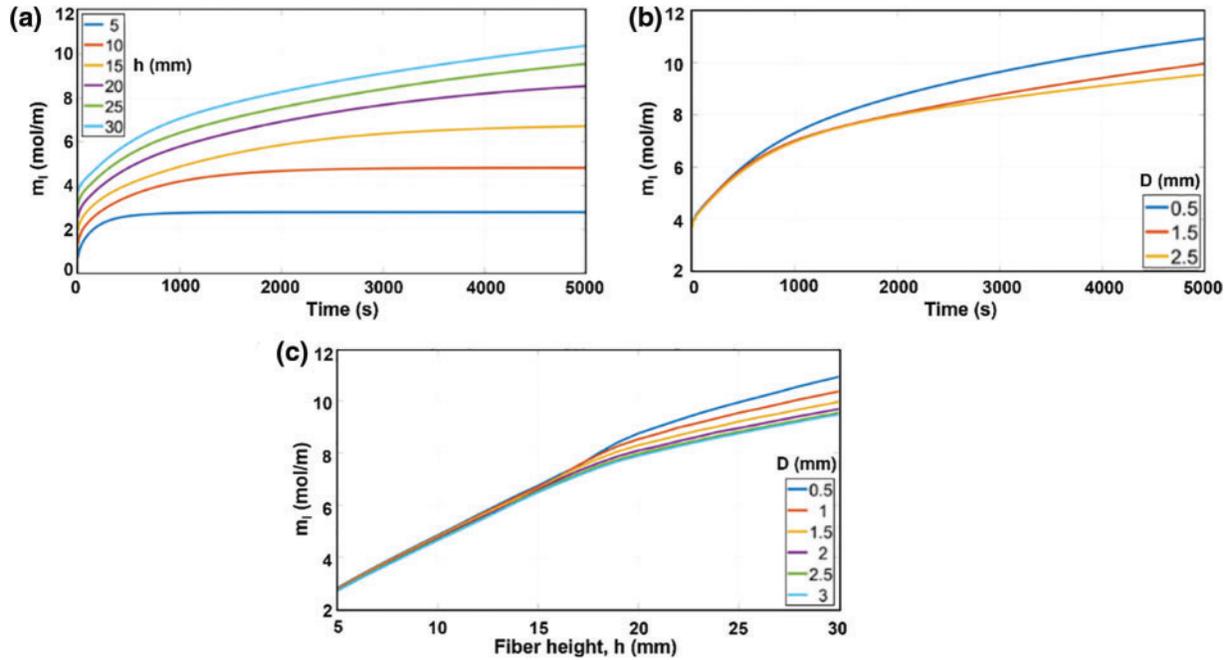
Figure 6: Vapor mass content in the fiber *vs.* time with varying (a) fiber heights (h = 5–30 mm), (b) distances between fibers (D = 0.5–2.5 mm), and (c) at t = 5000 s *vs.* the fiber height with varying inter-fiber distances (D = 0.5–3 mm)

Fig. 7 presents the vapor mass content per height in fiber for *vs.* time as a function of height, *vs.* time as a function of the distance between fibers, and for time of 5000 s as a function of height. As shown, the total mass content in fiber per height increases with time. The final values of mass per height decrease by an increase of height and the distance between them.

Fig. 8a presents the effect of inlet temperature on maximum temperature difference, ΔT, in the system (ΔT). As shown, less inlet temperature causes the higher temperature to increase even if the total change is not significant. Such dependence shows the still strong correlation with heat transfer linearly. For a sun radiation power less than 550 W/m², insignificant temperature differences were observed in the system regardless of the inlet (or ambient) temperature. As such, the ΔT results under $q_w < 400$ W/m² was excluded from Fig. 8a.

Fig. 8b presents the effect of sun radiation on the integral of evaporation in system. As shown by the increase of sun radiation, the evaporation rate increases nearly linearly. Such dependence shows the still strong correlation between the evaporation rate and heat input in the fiber bundles.
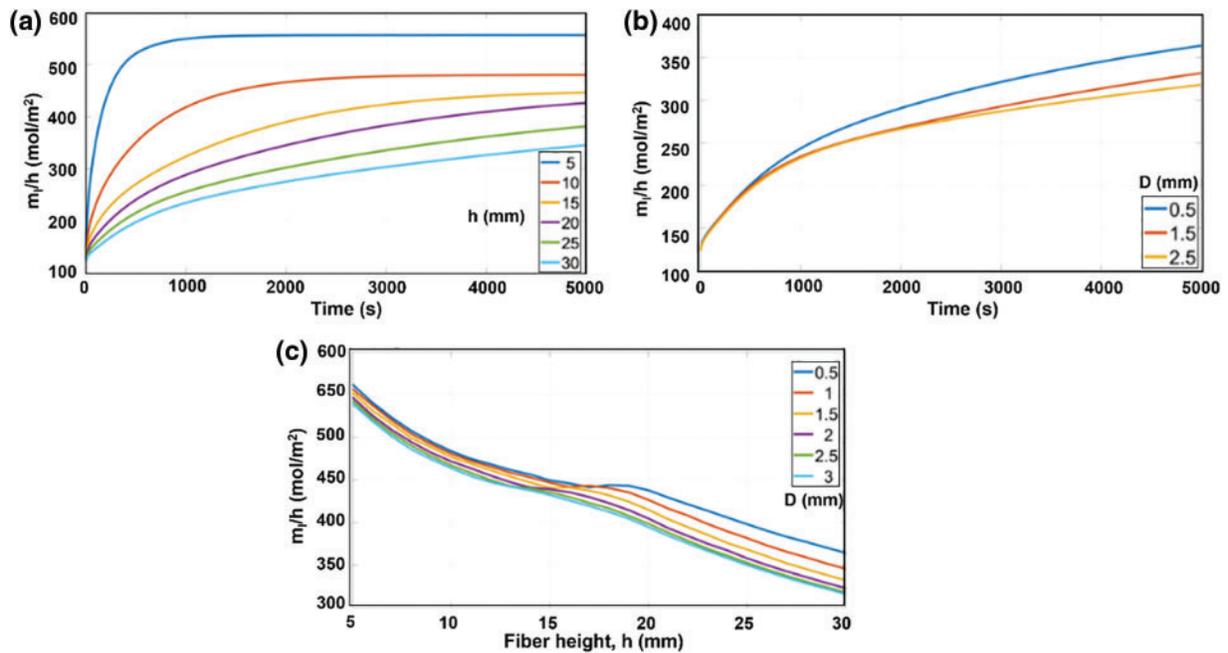
Figure 7: Vapor mass content per height within the fiber (a) *vs.* time as a function of height, (b) *vs.* time as a function of distance between fibers, (c) for time of 5000 s as a function of height
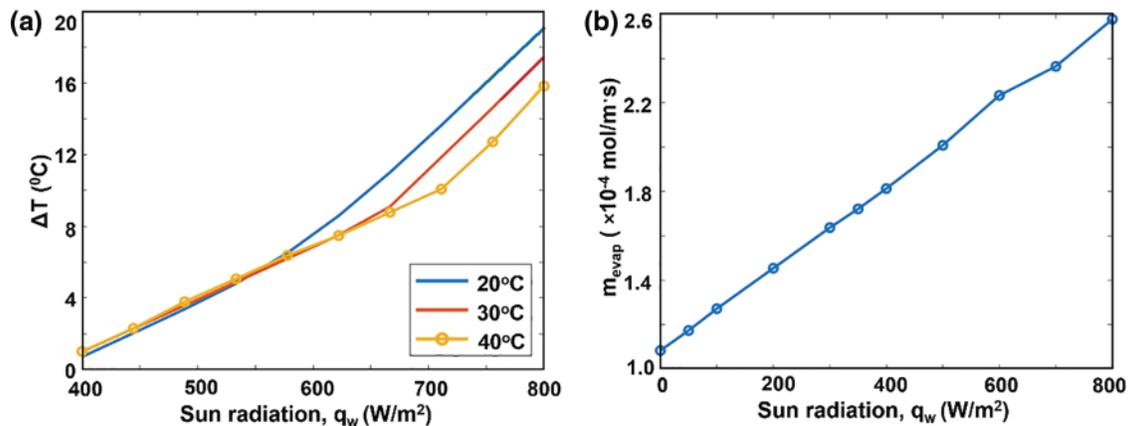
Figure 8: Sun radiation effect on vapor evaporation rate: (a) effect of inlet temperature to maximum temperature difference (ΔT); and (b) effect of sun radiation on integral of evaporation in system

4 Discussion

Using COMSOL-based computational model two-dimensional fibers porous fibers, this study investigates how solar vapor is generated when the fibers are evaporating based on their height and distance from one another. Optimal design of porous media can improve the efficiency of solar vapor generators by enhancing the heat transfer process. Carbon fiber bundles can act as a highly conductive material that can efficiently transfer heat from the solar collector to the working fluid. Additionally,

the optimal design of porous media can reduce the overall size of the solar vapor generator, which can further reduce the cost of installation and operation.

The length of the fiber in an osmotic system can significantly affect its efficiency. Longer fibers can provide a larger surface area for water to diffuse through, which can increase the rate of water transport and improve the overall efficiency of the system (Figs. 4 and 5). However, longer fibers can also increase the resistance to flow and may require more energy to maintain the necessary pressure gradient. Therefore, the optimal fiber length will depend on various factors such as the membrane material, the concentration gradient, and the desired water flux rate.

The inter-fiber distance D was shown to have a nonlinear effect on the fiber bundle evaporation rate (Figs. 6 and 7). This parameter affected the density or packing of the fiber bundle, with a smaller D leading to a densely packed bundle. From Figs. 6 and 7, as long as $D \geq 1.5$ mm, the evaporation rate from a single fiber did not differ much. This observation can have an important implication on the fiber bundle design. Compared to a fiber bundle with an unnecessarily larger inter-fiber distance D, a fiber bundle with a smaller D means either a higher evaporation rate from the same area or the same evaporation rate from a smaller area. On the other hand, the evaporation rate decreases drastically when D is smaller than 1.5 mm (Figs. 6 and 7), indicating that a too densely packed fiber bundle can decrease the evaporation efficiency. As a result, an inter-fiber distance of 1.5 mm was recommended for the fiber bundle.

Air temperature has a mixed effect on the fiber bundle evaporation rate (Fig. 8). As air temperature increases, the molecules in the air gain more energy and move faster, which allows them to absorb more water vapor from the water surface. This leads to an increase in the rate of evaporation. However, at very high temperatures, the rate of evaporation may start to decrease due to factors such as increased humidity and reduced concentration gradient between the water surface and the air. Additionally, if the air temperature is too low, the rate of evaporation may be limited by the amount of energy available to break the bonds between water molecules. Overall, air temperature and velocity are important factors that affect the rate of evaporation, and understanding their effects can be useful for applications such as drying processes, cooling systems, and weather forecasting.

Limitations of this study included a finite number of fibers and 2D simulations. However, even with ten 2D fibers to simulate a fiber bundle using Multiphysics COMSOL, extensive computational resources were required, including large RAM, long simulation time, and multi-tetra storage. It was also noted that this numerical study aimed to investigate the feasibility and the expected rate of solar vapor generation; comparable experiments are lacking in the current literature and complementary experiments are needed to validate the results in this study.

5 Summary

A numerical study of solar vapor generation from fiber bundles was conducted by systematically varying the design and operation parameters such as fiber height, inter-fiber distance, ambient temperature, and sun radiation intensity. The main results from this study are summarized as follows:

- A decrease in humidity at the last fiber is caused by an increase in fiber height.
- Fiber bundles with shorter heights retain more water.
- The last fiber receives less humidity as the distance increases.
- Keeping the fiber bundles' water content is easier when the distance between them is shorter.
- With increasing height, the concentration of vapor on the surface decreases.

- On the surface, vapor concentration is constant, but after some height it suddenly decreases.
- Because of the heat received at the top of each bundle, evaporation rates are highest at the top.
- Mass values increased as the height increased and decreased as the distance between them increased.
- Increasing time results in an increase in the mass content in fiber per height.
- The time to reach the equilibrium varies with the fiber height, which ranges from 1000 s for a 5-mm fiber to 5000 s for a 30-mm fiber.
- As the height and the distance between them increase, the final values of mass per height decrease.
- The evaporation rate increases with increasing sun radiation.
- The evaporation rate increases with the increase in fiber height.
- A fiber bundle model with a fiber height of 15–20 mm and an inter-fiber distance of 1.5 mm is recommended for both enhanced performance and reduced cost.

References

1. Almasoud, A. H., Gandayh, H. M. (2015). Future of solar energy in Saudi Arabia. *Journal of King Saud University—Engineering Sciences, 27(2),* 153–157.

2. Bae, K., Kang, G., Cho, S. K., Park, W., Kim, K. et al. (2015). Flexible thin-film black gold membranes with ultrabroadband plasmonic nanofocusing for efficient solar vapour generation. *Nature Communications, 6,* 10103.

3. Bella, F., Galliano, S., Falco, M., Viscardi, G., Barolo, C. et al. (2017). Approaching truly sustainable solar cells by the use of water and cellulose derivatives. *Green Chemistry, 19(4),* 1043–1051.

4. Bella, F., Galliano, S., Falco, M., Viscardi, G., Barolo, C. et al. (2016). Unveiling iodine-based electrolytes chemistry in aqueous dye-sensitized solar cells. *Chemical Science, 7(8),* 4880–4890.

5. Brindle, I. D. (2020). Chapter 8—vapor generation. In: Beauchemin, D. (Ed.), *Sample introduction systems in ICPMS and ICPOES*, pp. 381–409. Amsterdam: Elsevier.

6. Chen, M., Li, G., Wang, Q., Zhu, Z., Jiang, Y. et al. (2022). Evaluation of solar energy transmission and heat-mass transfer in a floating solar concentrated distillation configuration. *Sustainable Energy Technologies and Assessments, 52(39),* 102327.

7. Ge, C., Song, Z., Yuan, Y., Song, B., Ren, S. et al. (2022). Solar steam generation by porous conducting polymer hydrogel. *Solar Energy, 240(11),* 237–245.

8. Ghasemi, H., Ni, G., Marconnet, A. M., Loomis, J., Yerci, S. et al. (2014). Solar steam generation by heat localization. *Nature Communications, 5(1),* 4449.

9. He, M., Alam, M. K., Liu, H., Zheng, M., Zhao, J. et al. (2021). Textile waste derived cellulose based composite aerogel for efficient solar steam generation. *Composites Communications, 28(25),* 100936.

10. He, M., Dai, H., Wang, L., Qin, X., Yu, J. (2022). Facile fabrication of polydopamine nano-sphere-decorated fabric for solar steam generation. *Textile Research Journal, 92(19–20),* 3451–3461.

11. He, P., Hao, L., Liu, N., Bai, H., Niu, R. et al. (2021). Controllable synthesis of sea urchin-like carbon from metal-organic frameworks for advanced solar vapor generators. *Chemical Engineering Journal, 423(12),* 130268.

12. Ito, Y., Tanabe, Y., Han, J., Fujita, T., Tanigaki, K. et al. (2015). Multifunctional porous graphene for high-efficiency steam generation by heat localization. *Advanced Materials, 27(29),* 4302–4307.

13. Kalogirou, S. A. (2005). Seawater desalination using renewable energy sources. *Progress in Energy and Combustion Science, 31(3),* 242–281.

14. Li, A., Xiong, J., Liu, Y., Wang, L., Qin, X. et al. (2022). Fiber-intercepting-particle structured MOF fabrics for simultaneous solar vapor generation and organic pollutant adsorption. *Chemical Engineering Journal, 428,* 131365.

15. Li, X., Ci, L., Kar, S., Soldano, C., Kilpatrick, S. J. et al. (2007). Densified aligned carbon nanotube films via vapor phase infiltration of carbon. *Carbon, 45(4),* 847–851.

16. Lim, H., Kim, M., Yoo, J., Lee, D., Lee, M. et al. (2022). Environmentally safe and renewable solar vapor generation device based on Prussian blue nanoparticles immobilized on cellulose nanofibers. *Desalination, 524,* 115477.

17. Linic, S., Christopher, P., Ingram, D. B. (2011). Plasmonic-metal nanostructures for efficient conversion of solar to chemical energy. *Nature Materials, 10(12),* 911–921.

18. Liu, K., Jiang, Q., Tadepalli, S., Raliya, R., Biswas, P. et al. (2017). Wood-graphene oxide composite for highly efficient solar steam generation and desalination. *ACS Applied Materials & Interfaces, 9(8),* 7675–7681.

19. Liu, K., Sun, Y., Chen, L., Feng, C., Feng, X. et al. (2008). Controlled growth of super-aligned carbon nanotube arrays for spinning continuous unidirectional sheets with tunable physical properties. *Nano Letters, 8(2),* 700–705.

20. Liu, Y., Liu, H., Xiong, J., Li, A., Wang, R. et al. (2022). Bioinspired design of electrospun nanofiber based aerogel for efficient and cost-effective solar vapor generation. *Chemical Engineering Journal, 427,* 131539.

21. Liu, Y., Yu, S., Feng, R., Bernard, A., Liu, Y. et al. (2015). A bioinspired, reusable, paper-based system for high-performance large-scale evaporation. *Advanced Materials, 27(17),* 2768–2774.

22. Ma, X., Jia, X., Yao, G., Wen, D. (2022). Umbrella evaporator for continuous solar vapor generation and salt harvesting from seawater. *Cell Reports Physical Science, 3(7),* 100940.

23. Majumder, M., Chopra, N., Andrews, R., Hinds, B. J. (2005). Nanoscale hydrodynamics: Enhanced flow in carbon nanotubes. *Nature, 438(7064),* 44.

24. Mizuno, K. E. A. (2009). A black body absorber from vertically aligned single-walled carbon nanotubes. *Proceedings of the National Academy of Sciences of the United States of America, 106(15),* 6044–6047.

25. Cancilla, N., Gurreri, L., Ciofalo, L., Cipollina, M., Tamburini, A. et al. (2023). Hydrodynamics and mass transfer in straight fiber bundles with non-uniform porosity. *Chemical Engineering Science, 279(11),* 118935.

26. Ni, G., Li, G., Boriskina, S. V., Li, H., Yang, W. et al. (2016). Steam generation under one sun enabled by a floating structure with thermal concentration. *Nature Energy, 1(9),* 16126.

27. Ni, G., Miljkovic, N., Ghasemi, H., Huang, X., Boriskina, S. V. et al. (2015). Volumetric solar heating of nanofluids for direct vapor generation. *Nano Energy, 17,* 290–301.

28. Ouyang, X., Wu, P., Deng, J., Ma, Q., Dong, X. et al. (2022). Flexible solar absorber using hydrophile/hydrophobe amphipathic Janus nanofiber as building unit for efficient vapor generation. *Separation and Purification Technology, 297(6),* 121526.

29. Sun, Y., Fan, L., Lin, X., Feng, C., Peng, S. et al. (2022). Porous biomass foam of polypyrrole-coated cattail fibers for efficient photothermal evaporation. *Industrial Crops and Products, 178,* 114559.

30. Yao, G., Feng, Y., Liu, G., Xu, J. (2020). Solar vapor generation using bubbly flow nanofluids with collaborative light-harvesting nanoparticles. *Solar Energy, 207(19),* 1214–1221.

31. Yin, Z., Wang, H., Jian, M., Li, Y., Xia, K. et al. (2017). Extremely black vertically aligned carbon nanotube arrays for solar steam generation. *ACS Applied Materials and Interfaces, 9(34),* 28596–28603.

32. Yu, S., Zhang, Y., Duan, H., Liu, Y., Quan, X. et al. (2015). The impact of surface chemistry on the performance of localized solar-driven evaporation system. *Scientific Reports, 5(1),* 13600.

33. Zang, L., Finnerty, C., Zheng, S., Conway, K., Sun, L. et al. (2021). Interfacial solar vapor generation for desalination and brine treatment: Evaluating current strategies of solving scaling. *Water Research, 198(29),* 117135.

34. Zhang, Q., Yang, X., Deng, H., Zhang, Y., Hu, J. et al. (2022). Carbonized sugarcane as interfacial photothermal evaporator for vapor generation. *Desalination, 526,* 115544.

35. Zhang, R., Ning, Z., Zhang, Y., Zheng, Q., Chen, Q. et al. (2013). Superlubricity in centimeters-long double-walled carbon nanotubes under ambient conditions. *Nature Nanotechnology, 8(12),* 912–916.

36. Zhang, X., Jiang, K., Feng, C., Liu, P., Zhang, L. et al. (2006). Spinning and processing continuous yarns from 4-inch wafer scale super-aligned carbon nanotube arrays. *Advanced Materials, 18,* 1505–1510.

37. Zhang, Y., Zou, G., Doorn, S. K., Htoon, H., Stan, L. et al. (2009). Tailoring the morphology of carbon nanotube arrays: From spinnable forests to undulating foams. *ACS Nano, 3(8),* 2157–2162.

38. Zhao, G., Chen, Y., Pan, L., Chen, B., Ren, L. et al. (2022). Plant-inspired design from carbon fiber toward high-performance salt-resistant solar interfacial evaporation. *Solar Energy, 233(8),* 134–141.

39. Corpart1, M., Dervaux, J., Poulard, C., Restagno, F., Boulogne, F. (2022). Evaporation of liquid coating a fiber. *Europhysics Letters, 139(4),* 43001.

40. Lim, O., Ahn, T. (2019). Fiber-optic measurement of liquid evaporation dynamics using signal processing. *Journal of Lightwave Technology, 37(19),* 4967–4975.

41. Li, T., Fang, Q., Wang, J., Lin, H., Han, Q. et al. (2021). Exceptional interfacial solar evaporation via heteromorphic PTFE/CNT hollow fiber arrays. *Journal of Materials Chemistry A, 9(1),* 390–399.